Fuel 285 (2021) 118955

Contents lists available at ScienceDirect

Fuel

journal homepage: www.elsevier.com/locate/fuel

Phenomenological micro-pilot ignition model for medium-speed dual-fuel engines

Hyunchun Park[a,e,*], Yuri M. Wright[a,b], Omar Seddik[a], Ales Srna[d], Panagiotis Kyrtatos[c], Konstantinos Boulouchos[a]

[a] ETH Zürich, Laboratory for Aerothermochemistry and Combustion Systems, Switzerland
[b] Combustion & Flow Solutions GmbH, Switzerland
[c] Vir2sense GmbH, Switzerland
[d] University of New South Wales, Engine Research Laboratory, Australia
[e] Hyundai Heavy Industries Co., Ltd., Republic of Korea

ARTICLE INFO

Keywords:
Dual-fuel engines
Ignition modeling
Micro-pilot spray
Micro-pilot ignition
Phenomenological model

ABSTRACT

The medium-speed dual-fuel engine has become popular in the marine industry for its advantages of fulfilling the stringent emission regulations and relative affordability of natural gas. In such engines, the ignition process importantly influences the subsequent combustion processes and engine performance. This work developed a phenomenological micro-pilot ignition model with a minimal number of tuning parameters aiming to improve the understanding of the ignition event and enable better control of the dual-fuel engine. The model comprises of a spray and a chemistry submodel to accurately capture the interaction between the direct injection of a small amount of diesel fuel (called micro-pilot) and a two-stage ignition of the diesel fuel mixed with the surrounding reactive charge in relatively low temperature. A 1D transient spray model is adapted to reproduce the micro-pilot spray characteristics by assuming a realistic trapezoidal fuel injection profile and the varying discharge coefficient during the transient spray period. The chemical reactions are modeled with a 0D transient flamelet approach based on an opposed flow reactor. The model is validated using three sets of experimental data, namely ECN Spray A (constant volume chamber), RCEM with optical accessibility, and finally, medium-speed dual-fuel engine. Quantitatively good predictions of the spray formation, ignition delay, and ignition location over broad conditions ranging from the conventional diesel ignition to the micro-pilot ignition in the dual-fuel engine are demonstrated. Finally, the developed model is used to explore the characteristics of micro-pilot ignition under conditions relevant to the medium-speed dual-fuel engines.

1. Introduction

In recent years, the medium-speed dual-fuel(DF) engine has become popular in the marine industry. DF engines can be operated with either diesel or natural gas fuel, which brings various advantages in terms of emissions, fuel economy, and redundancy [1]. In particular, using natural gas can significantly reduce CO2, NOx, SOx, and particulate matter emissions without using any additional after-treatment system helping fulfill the stringent emission regulations. However, this combustion mode also faces challenges with CH4 and UHC emissions, which are higher than those of diesel engines [2,3].

Most medium-speed DF engines are developed based on the diesel engine. Therefore, these engines can usually operate in diesel mode with similar combustion characteristics as conventional diesel engines. On the other hand, the gas mode exhibits unique combustion characteristics. The combustion in gas mode is a highly complex phenomenon as it includes characteristics of both diffusion and premixed combustion. The ignition of the premixed main charge containing the gaseous fuel (more than 98% of the total fuel energy) takes place through the direct injection of a small amount of diesel fuel (usually 0.5 to 2% of the total fuel energy), which is often called micro-pilot (MP) injection. This MP injection of diesel fuel initiates the autoignition and the initial diffusion combustion, while the subsequent combustion of the surrounding charge occurs in a premixed mode.

The ignition process is crucial in DF engines since it governs the subsequent combustion processes and the engine performance [4]. Despite the numerous studies on conventional diesel ignition, the ignition in DF engines still needs further investigations since it is different

* Corresponding author at: ETH Zürich, Laboratory for Aerothermochemistry and Combustion Systems, Switzerland.
E-mail address: phc0112@lav.mavt.ethz.ch (H. Park).

https://doi.org/10.1016/j.fuel.2020.118955
Received 19 May 2020; Received in revised form 28 July 2020; Accepted 10 August 2020

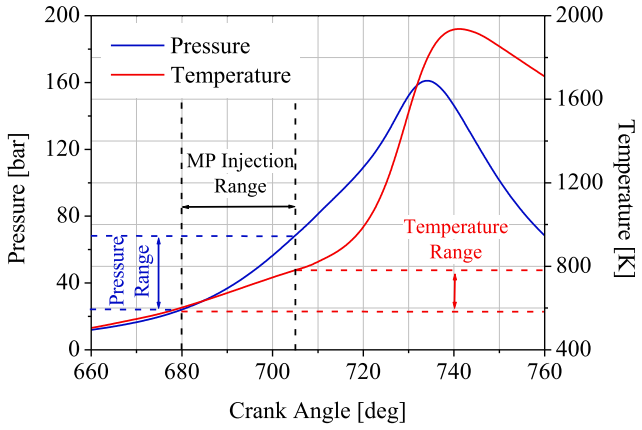

Fig. 1. Pressure and temperature traces of a typical medium-speed DF engine (see the specifications in [13]).

in many aspects. The compression ratio of DF engines is typically reduced to suppress abnormal combustion, such as knocking and pre-ignition [5]. As shown in Fig. 1, this results in a low in-cylinder gas temperature of less than 800 K during MP injection in typical medium-speed DF engines. In this temperature range, the diesel ignition is known to be profoundly affected by low temperature (LT) reactions, and thus often called two-stage ignition [6,7]. Also, several studies have shown that the background methane mixture is inhibiting the ignition [8,9]. Thus, contrary to the conventional diesel engines, the ignition delay in the DF engine is usually longer than the MP injection duration. This adds to the complexity of the ignition phenomena in DF engines since the ignition is affected by not only the chemical reactions but also the spatial distribution of the transient diesel spray [4,10–12].

These specific characteristics of ignition in DF engines highlight the need for a sophisticated MP ignition model to improve the understanding of the underlying processes and to enable better control of the combustion event. There have been several modeling studies of MP ignition recently. The most involved models use a multi-dimensional (CFD) analysis to calculate the spray distribution on a fine-mesh using well-known spray models. Then, ignition is calculated by using either detailed chemical mechanisms for each cell [14–16], pre-tabulated ignition progress along with the mixture conditions [17], or a tuned Arrhenius type correlation with average temperature and equivalence ratio terms [18]. The less involved models use a quasi-dimensional analysis and, various MP ignition models have been developed. The empirical Wiebe model based on measured data is often used for its simplicity [13,19]. For specific cases, such as low-speed 2-stroke engines, a tabulated ignition delay model based on homogeneous reactor calculation is often employed neglecting MP spray conditions [20]. While in other models, the 1D transient spray model [21] is employed to deal with the transient MP injection because of the particularly short injection duration. In some of these models, the ignition delay is calculated only at the spray tip, assuming that the richest region is the most reactive [22], or the ignition delay is estimated by tracking the reactivity propagation within the whole spray envelope [23]. Yet another approach to the MP ignition model applies the spray parcels. Here, ignition integrals based on tabulated ignition delay of each parcel are used to calculate the ignition delay [24–26]. Despite the recent advantages in computational power, the multi-dimensional CFD analysis is still expensive for multi-objective DF engine optimization or combustion control in particular. This is further exacerbated by the more numerous operating parameters in DF engines relative to the conventional diesel engines. Hence, quasi-dimensional analysis is still needed for DF engine optimization [27] and parametric studies of operating conditions [28].

In this paper, a novel phenomenological MP ignition model for a medium-speed DF engine is developed, and its performance is assessed in three steps. First, the MP ignition model composed a 1D transient spray submodel, and a novel chemistry submodel is introduced. The spray submodel is tailored to accurately capture the behavior of the short MP spray with particular attention. For that purpose, the realistic trapezoid fuel injection profile, the transient evolution of the discharge coefficient, and a term for the momentum-dissipation due to turbulence are introduced to the spray model. The chemistry submodel using the 0D flamelet model based on the opposed flow reactor is adapted, which is often used for the combustion analysis using CFD [17,29]. This model is novel for simulating the MP ignition since it can account for the interaction between the spray and chemistry, which is especially important in the short MP spray. Second, the developed model and submodels are validated using a set of experimental data ranging from the conventional diesel ignition (ECN Spray A), the MP ignition in an optically accessible rapid compression and expansion machine (RCEM), and finally, an MP ignition in medium-speed DF engines. The MP ignition model requires tuning for the injector nozzle related coefficients only, which are reflecting the geometric characteristics of the specific injector nozzle. Other parameters are set to constant values even for different cases from the relatively simple ECN spray A to the more sophisticated medium-speed DF engine. The developed MP ignition model with a minimal number of tuning parameters shows good agreements with the various measurement campaigns, especially for the ignition delay and ignition location. Finally, the validated MP ignition model is used to investigate the characteristics of ignition in medium-speed DF engines for numerous parametric variations such as the start of injection (SOI), the duration of injection (DOI), and the air-to-methane ratio of background mixture.

2. Model description

The MP ignition model consists of a spray model and a chemical reaction model. First, the calculation domain is determined. Since the primary purpose of the MP ignition model is to predict the ignition delay and location precisely, the temporal calculation range is set from the start of MP injection until the model predicted ignition. The spatial calculation range is determined based on the preliminary estimation of the spray penetration using a relatively simple steady-state spray model from Naber and Siebers [30] using the conditions at SOI. The model domain length of 1.5 times the preliminary penetration distance from the injector orifice is assumed. The time step and mesh size are determined to keep the Courant number below 0.5. The inputs required for the ignition model are the conditions within the combustion chamber (temperature, pressure, composition, turbulence intensity) and the MP spray properties (rate of injection, injector specifications, injection timing, injection duration, injection pressure). A well-established 1D transient spray model from Musculus and Kattke [21] is employed as the base model. Various improvements are applied to the spray model to accurately predict the spray characteristics with a particular focus on the MP spray, as described in section 2.1. The chemical reaction model employs a 0D flamelet model designed for the opposed flow reactor with the appropriate detailed chemical mechanisms, which is chosen in section 2.2. The submodels are coupled through the inputs to the 0D flamelet calculation, which are obtained from the spray submodel and combustion chamber conditions. The outputs of the model are the ignition delay and ignition location.

2.1. Spray model – Formulation

The two most significant differences in spray formation between diesel and DF engines are that the MP spray in the DF engine is injected into lower ambient temperature, and it has a significantly short injection duration. This causes MP ignition to behave quite differently from diesel ignition. In diesel engines, the mean spray temperature distribution along the spray axis before ignition is similar to the long injection duration case shown in Fig. 2. The mean spray temperature is

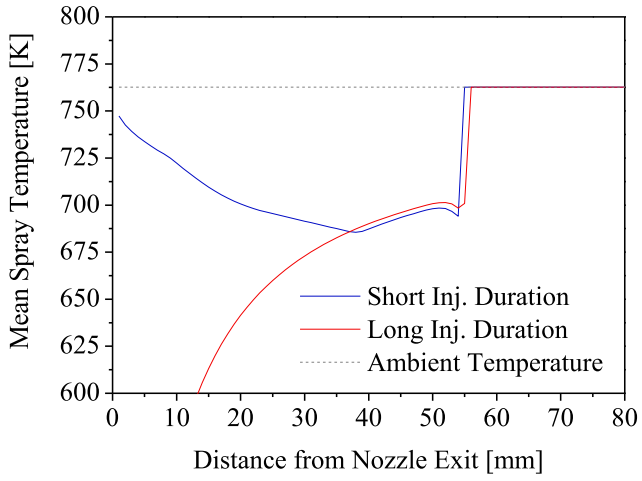

Fig. 2. Volume averaged spray temperature distribution along the axis from the nozzle exit for different injection durations.

lowest at the nozzle exit where the injected fuel evaporates, and the spray temperature gradually increases toward the spray tip as the fuel is mixed with the surrounding charge. Therefore, the ignition, mostly affected by temperature and residence time, is known to occur in the spray tip region.

On the other hand, in the DF engine, the temperature distribution along the spray axis before ignition follows the evolution like in the short injection duration case in Fig. 2. Since the ignition delay in DF engines is usually longer than the fuel injection duration, the mixing of fuel with the surrounding charge accelerates immediately after the end of fuel injection in the trailing edge of the spray near the nozzle exit [21]. Therefore, the highest temperature region of the spray can be either the nozzle exit or spray tip, while the middle of the spray along the axis has a lower temperature. In such temperature distribution, the MP ignition can occur not only at the spray tip but also at the appropriate point upstream of the spray tip. Consequently, the MP ignition model requires a spray model showing the spray characteristics not only at the spray tip but also the entire spray envelope.

The MP spray formation is modeled using the 1D transient spray model by Musculus and Kattke [21]. This model assumes a fully developed spray with a conical shape, as shown in Fig. 3. Governing equations for mass conservation (1) and momentum conservation (2) are solved along the spray axis discretized into cone-shaped 1D control volumes. This well-established model is extended to capture the momentum dissipation due to turbulence characteristic of engines (term in Eq. (2), further described in the following). In addition, particular attention is paid to the model inputs to capture the specific characteristics of the MP spray accurately as well as to minimize the number of tuning parameters. Therefore, the spray cone angle (θ) is estimated using an empirical correlation (3) [31] and tuned via the appropriate value (C_{sa}) for each injector nozzle, making the C_{sa} the only tuning parameter in the model. The velocity and fuel volume fraction distributions are assumed to be fully developed, and they are modeled as in Eq. (4) [32] with the value of α set to 1.5 (for this value, β is given as 2.02). Also, the central value of the assumed profile can be expressed by Eq. (5). Further details of the spray model can be found in [21,33].

$$m_{fuel,i}^{t+1} = m_{fuel,i}^{t} + \rho_{fuel}\left[(\beta \bar{X}_{fuel}\bar{u}A)_{i-1}^{t} - (\beta \bar{X}_{fuel}\bar{u}A)_{i}^{t}\right]\Delta t \tag{1}$$

$$M_{i}^{t+1} = M_{i}^{t} + \left[(\bar{\rho}\beta\bar{u}^{2}A)_{i-1}^{t} - (\bar{\rho}\beta\bar{u}^{2}A)_{i}^{t}\right]\Delta t - C_{TKE,loss}\, m_{i}^{t}\,(\bar{u}_{i}^{t}/R_{i})\sqrt{(2/3)k\Delta t} \tag{2}$$

$$\tan(\theta/2) = C_{sa}\left[(\rho_{charge}/\rho_{fuel})^{0.19} - 0.0043\sqrt{\rho_{charge}/\rho_{fuel}}\right] \tag{3}$$

$$X_{fuel} = \left[1 - (r/R)^{\alpha}\right]^{2} X_{fuel,center} \tag{4}$$

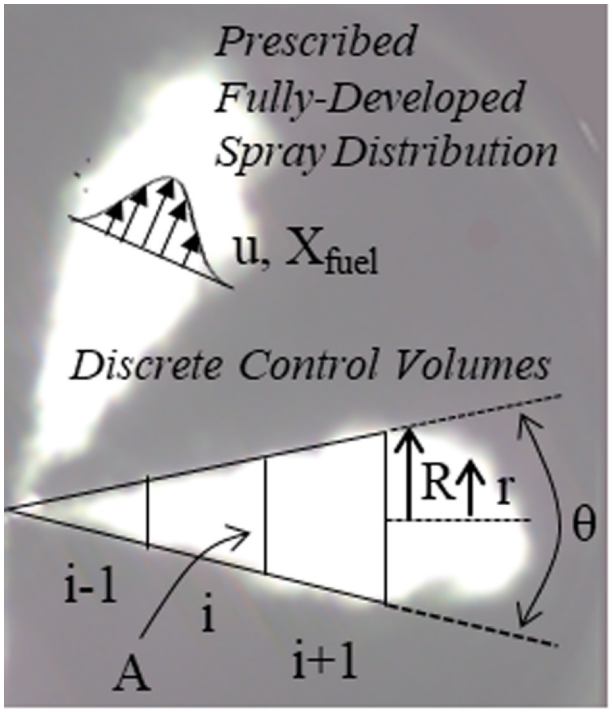

Fig. 3. Schematic description of 1D transient spray model drawn over the visualized MP spray.

$$X_{fuel,center} = \bar{X}_{fuel}\left[(\alpha + 1)(\alpha + 2)\right]/\alpha^{2} \tag{5}$$

The remainder of this section describes the spray model validation. The rate of injection and spray penetration are measured in a constant volume chamber experiment under the non-reactive DF engine-like conditions [34]. The spray measurements are done using an MP injector from a medium-speed DF engine under test conditions that resemble those at the MP SOI, the ambient density of 25 kg/m^3, the injection pressure of 1000 bar, and injection duration of 1msec. In diesel engines, the rate of injection (ROI) is often modeled as a rectangle due to its relatively long injection duration. However, due to the short injection duration, the MP spray is thoroughly affected by the transition periods at the start and end of injection, which are often called ramp-up and ramp-down transients. Therefore, the approximation of the ROI with a rectangle may distort the measured ROI [34] over the entire injection duration, as shown in Fig. 4. Eventually, this leads to poor predictions of the spray penetration and temperature distribution by the spray model, as shown in Fig. 5 and Fig. 6, respectively. This influences the model prediction of the ignition event as well. That is why the ROI of MP spray is approximated to have a trapezoid shape to catch the spray characteristics during the transition period.

The boundary conditions at nozzle exit should be set carefully to estimate the spray characteristics during the transition period correctly. The model calculates the injection velocity and injection area at the injector nozzle exit according to the Bernoulli equation. To capture the transient injection rate, either the velocity coefficient ($C_{velocity}$) (6) or contraction coefficient (C_{area}) (7) can be tuned considering the actual flow through the nozzle. In the absence of a specific evolution model of these coefficients, the transition period can be handled by either keeping the contraction coefficient with a constant value and varying the velocity coefficient according to the ROI or vice versa.

$$A_{exit,actual} = C_{area}\cdot A_{exit} \tag{6}$$

$$u_{exit,actual} = C_{velocity}\cdot u_{exit} \tag{7}$$

During the transition period, when the needle of the injector opens or closes, a high-velocity gradient of fuel is formed at the nozzle inlet

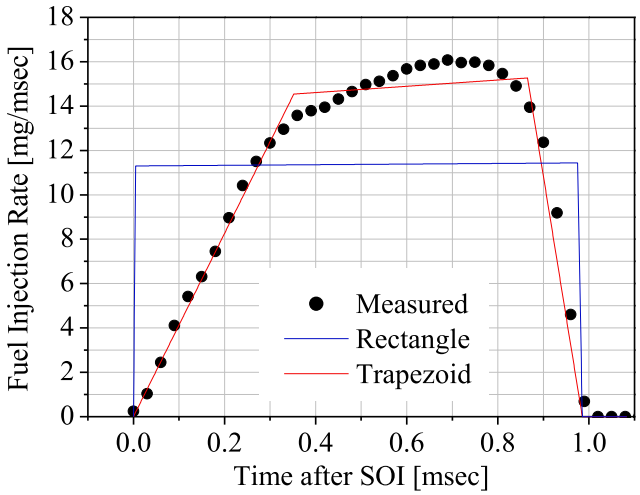

Fig. 4. Rate of injections for medium-speed DF engine measured in constant volume chamber under the conditions of ambient density of 25 kg/m^3, injection pressure of 1000 bar, and injection duration of 1msec, compared to the rectangle and trapezoid estimations.

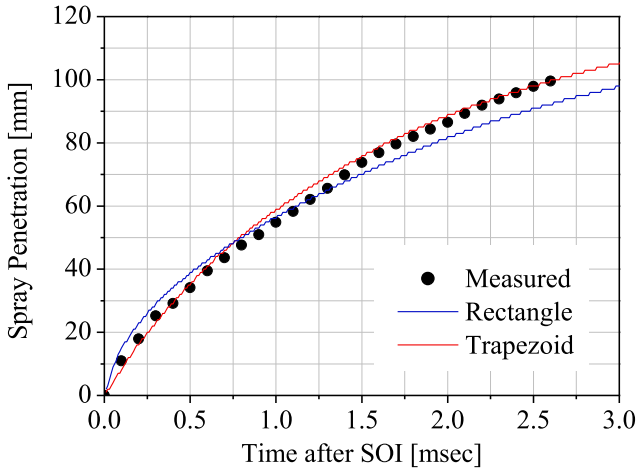

Fig. 5. Spray penetration predicted using different approximations of the rate of injection shapes, compared to experimental data measured in constant volume chamber under the conditions of ambient density of 25 kg/m^3, injection pressure of 1000 bar, and injection duration of 1msec.

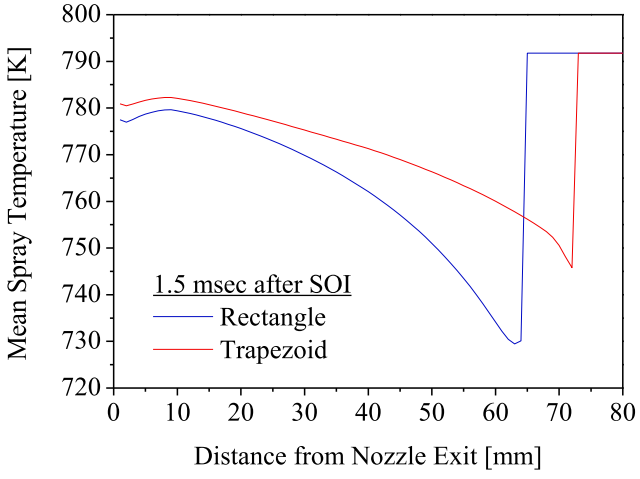

Fig. 6. Mean spray temperature prediction by the developed spray model for a different rate of injection shapes.

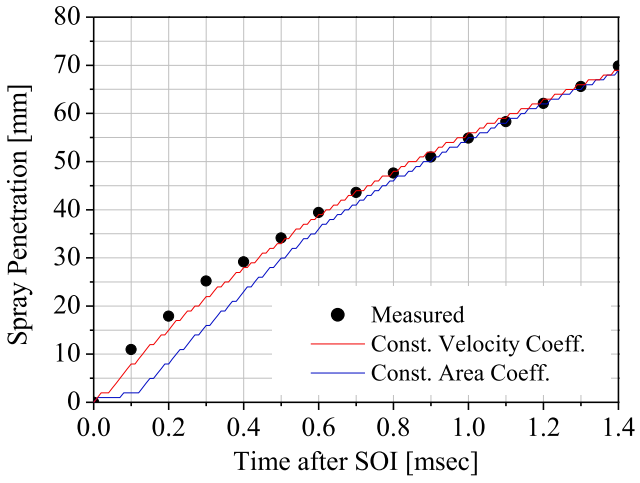

Fig. 7. Spray penetration comparison for a different interpretation of flow coefficient on 1D spray model (measured in constant volume chamber under the conditions of ambient density of 25 kg/m^3, injection pressure of 1000 bar, and injection duration of 1msec).

leading to cavitation often occurring inside the nozzle. This reduces the effective nozzle exit area while keeping the nozzle exit velocity above a specific value [35,36]. Therefore, the spray model adopts a method of fixing the velocity coefficient to a constant value and varying the contraction coefficient according to the ROI. With this assumption, the model reproduces the measured spray penetration with better accuracy, as in Fig. 7. However, the other method shows the lower spray penetration at SOI since it estimates nozzle exit velocity almost equal to zero in this region.

The spray model is further extended by a term accounting for turbulence effects on spray mixing and ignition in (2). Unlike the constant volume chamber, the flow within the combustion chamber of an engine is turbulent due to the intake flow, squish flow, and compression. This turbulent flow is known to have an impact on spray characteristics [37]. 3D CFD is used to quantify the effect of turbulence and validate the 1D spray model predictions. In CFD, the KH-RT spray breakup model and standard k-ε turbulence model are employed, And the turbulence is diversified by changing the values of initial turbulent kinetic energy (TKE). As shown in Fig. 8, higher TKE decreases spray penetration by dispersing the momentum of the spray. Thus, the momentum loss term due to the turbulence is added at the momentum conservation

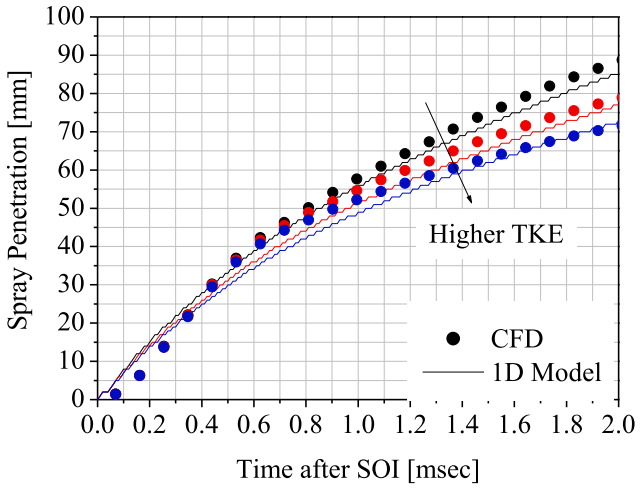

Fig. 8. Spray penetration for different turbulent kinetic energy levels (simulated under the conditions of ambient density of 25 kg/m^3, injection pressure of 1000 bar, and injection duration of 1msec).

Eq. (2). The term is designed to have a higher loss value when the turbulence gets stronger, and the velocity gradient in the radial direction gets higher. The term has a tuning parameter ($C_{TKE,loss}$), which is tuned to 0.75 to match the CFD predictions. The spray model with turbulence loss term predicts the spray penetration with precision, as shown in Fig. 8.

In the next stage, the 1D spray model is extended to calculate the scalar dissipation rate (SDR), which is a required input for the chemical reaction model besides the mixture fraction (Z). The mixture fraction can be obtained from the modeled fuel mass fraction through (8) by applying the fuel mass fraction at the fuel side (Y_{fuel}^0) equals one in the engine condition and using (11). The SDR is modeled by (12) assuming unity Lewis number [38]. Here, the local gradient of mixture fraction is calculated as (13) for the axial direction and as (14) for the radial direction. Then, the area-averaged SDR along the stoichiometric boundary of the spray for each time is calculated using (15). Finally, the area-averaged SDR for each mixture fraction is modeled using (16) by applying the stoichiometric SDR obtained from (15) [39].

$$Z = [1/(1+\phi_{mix})](\phi_{mix} Y_{fuel}/Y_{fuel}^0 - Y_{oxi}/Y_{oxi}^0 + 1) = Y_{fuel} \tag{8}$$

$$Y_{fuel} = \rho_{fuel} X_{fuel}/[\rho_{fuel} X_{fuel} + \rho_{charge}(1 - X_{fuel})] \tag{9}$$

$$\phi_{mix} = s Y_{fuel}^0/Y_{oxi}^0 \tag{10}$$

$$Y_{oxi} = Y_{oxi}^0(1 - Y_{fuel}) \tag{11}$$

$$\chi = 2D(\partial Z/\partial x_i)^2 = 2C_{diff} k_{cond}/(\rho c_P)(\partial Z/\partial x_i)^2 \tag{12}$$

$$\partial Z/\partial x = \rho_{fuel}\rho_{charge}/[\rho_{fuel} X_{fuel} + \rho_{charge}(1 - X_{fuel})]^2 \partial X_{fuel,center}/\partial x \tag{13}$$

$$\partial Z/\partial r = 2\alpha[(r/R)^{2\alpha-1} - (r/R)^{\alpha-1}]\rho_{fuel}\rho_{charge}/[\rho_{fuel} X_{fuel} + \rho_{charge}(1 - X_{fuel})]^2 X_{fuel,center} \tag{14}$$

$$\chi_{st.,avr} = \frac{\int (A_{st.,radial}\chi_{st.,radial} + A_{st.,LE}\chi_{st.,LE} + A_{st.,TE}\chi_{st.,TE})}{\int (A_{st.,radial} + A_{st.,LE} + A_{st.,TE})} \tag{15}$$

$$\chi = \chi_{st.,avr}(Z/Z_{st.})^2[\ln(Z/Z_{max})/\ln(Z_{st.}/Z_{max})] \tag{16}$$

The model performance is validated against the CFD results. For this purpose, the maximum mixture fraction (Z_{max}) and area-averaged SDR at stoichiometric locations ($\chi_{st.,avr}$) within the spray plume are compared. Three MP spray conditions with different injection timing or injection duration in medium-speed DF engines are used for validation. For each condition, Z_{max} and $\chi_{st.,avr}$ are well-matched with the CFD result, as shown in Fig. 9 and Fig. 10, except for the period just after the start of injection where the 1D spray model shows higher values than the CFD. These deviations are because the 1D spray model assumes the injected liquid fuel is fully evaporated just after the SOI. However, the liquid fuel needs time for evaporation in the CFD. Also, the reason for the highly fluctuating SDR in Fig. 10 is that the mesh used in the 1D spray model is coarser than the CFD mesh.

2.2. Chemical reaction model

The chemical reaction is modeled employing the transient flamelet approach [40], assuming the ignition in an MP spray can be modeled as a non-premixed opposed flow reactor. In addition, the interaction between the turbulence and chemical reaction also can be captured using flamelet equations (17), (18), which are solved in the mixture fraction space to predict the ignition delay and ignition locations. The boundary conditions are set as follows: for the oxidizer side, average pressure, temperature, and charge composition conditions within the cylinder are used. For the fuel side, fuel temperature is set constant. The cooling effect of the fuel evaporation is assumed negligible, especially for DF engines, since the injected fuel amount is tiny, and the ignition delay is

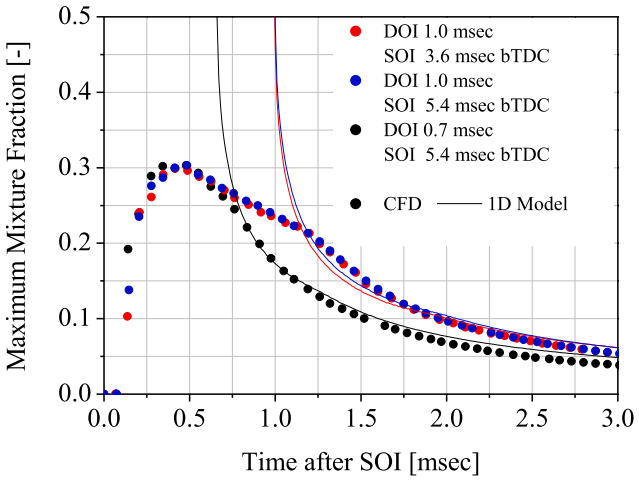

Fig. 9. Comparison of CFD and 1D spray model prediction of the maximum mixture fraction within the spray envelope for various MP SOI and MP DOI (simulated under the conditions of ambient density of 25 kg/m^3, and injection pressure of 1000 bar).

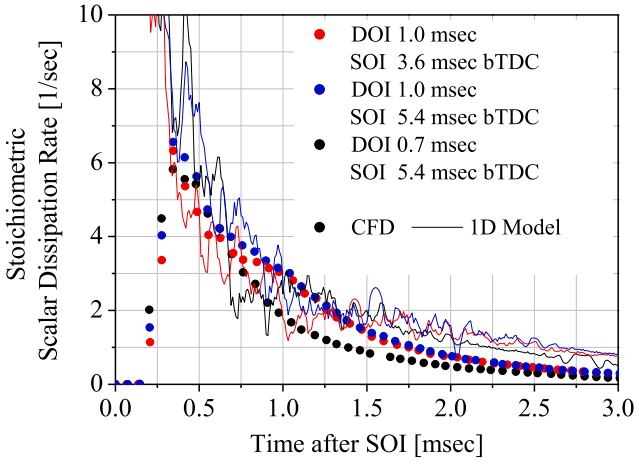

Fig. 10. Comparison of CFD and 1D spray model prediction of the area-averaged scalar dissipation rate at the stoichiometric location within the spray plume for various MP SOI and MP DOI (simulated under the conditions of the ambient density of 25 kg/m^3, and injection pressure of 1000 bar).

long enough to make fuel over-mixed with the surrounding charge. The transient values of the area-averaged SDR obtained from the spray model is used as a boundary condition characterizing the interaction between the turbulence and chemical reaction. The ignition events are defined based on the temperature increase for simplicity. The low-temperature (LT) ignition is defined as a 100 K temperature increase at each mixture fraction; this threshold value is found to correspond well to the sudden increase of CH_2O species. The high-temperature (HT) ignition is defined as a 500 K temperature increase for each mixture fraction, which corresponds to the sudden increase of OH species.

$$\rho\partial Y_k/\partial t = \dot{\omega}_k + 0.5\cdot\rho\chi\partial^2 Y_k/\partial Z^2 \tag{17}$$

$$\rho\partial T/\partial t = \dot{\omega}_T + 0.5\cdot\rho\chi\left(\partial^2 T/\partial Z^2 + (1/c_P)(\partial c_P/\partial Z)(\partial T/\partial Z) + \partial T/\partial Z\sum_{k=1}^{N}(1 - c_{P,k}/c_P)\partial Y_k/\partial Z\right) \tag{18}$$

The gaseous fuel in the charge mixture is modeled as pure methane, while n-heptane and n-dodecane are considered as surrogates for diesel

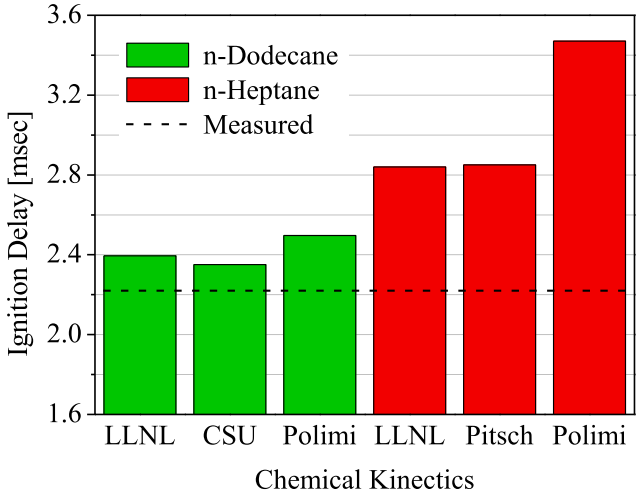

Fig. 11. Ignition delay comparisons for different surrogate fuels and chemical mechanisms (conditions relevant to the base case of the medium-speed DF engine – P_{SOI}: 49 bar, T_{SOI}: 725 K, DOI: 1msec, λ_{CH4}: 1.9, see section 3.3).

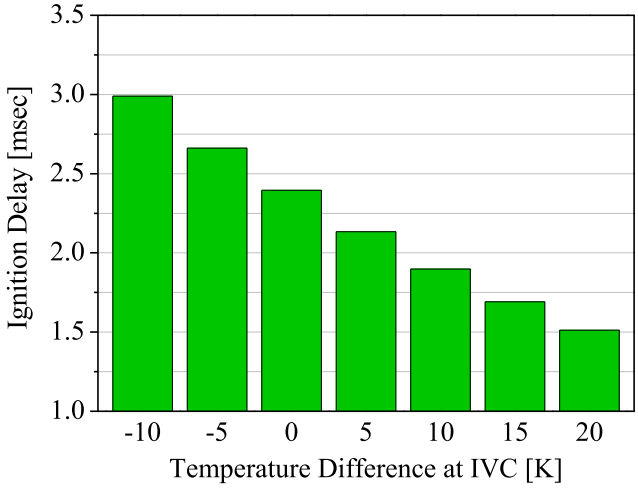

Fig. 12. Ignition delay prediction for a variation of the in-cylinder temperature at IVC (calculations are conducted for the base case of the medium-speed DF engine – P_{SOI}: 49 bar, T_{SOI}: 725 K, DOI: 1msec, λ_{CH4}: 1.9, see section 3.3).

fuel. Various chemical kinetic models for each diesel fuel surrogate candidate are tested to determine the chemical kinetic scheme most suitable for the MP ignition model developed. For n-heptane, chemical mechanisms of LLNL [41], Pitsch [42], and Polimi [43] are compared. For n-dodecane, chemical mechanisms of LLNL [44], CSU [45], and Polimi [43] are compared. Finally, the N-dodecane modeled by the chemical mechanism of LLNL is chosen for efficiency and its compact size (163 species and 887 reactions) based on the precision of the ignition delay prediction when compared to the measurement, as shown in Fig. 11.

3. Model validation and discussion

This section presents the MP ignition model validation using various test data. Additionally, the ignition characteristics of each case are investigated with the MP ignition model to highlight the underlying processes governing the ignition. First, the conventional diesel ignition is investigated using the data from the ECN Spray A tests. Then, the MP ignition is investigated using the data from ETH RCEM tests. Both experimental datasets include optical measurement data, which are compared to the model predictions as well. Finally, the MP ignition model is validated using the data from the multi-cylinder medium-speed DF engine test data.

Before validation, the MP ignition model requires tuning for the injector nozzle related coefficients only for each case, such as the spray cone angle coefficient, nozzle contraction coefficient, and nozzle velocity coefficient. These coefficients are reflecting the geometric characteristics of the specific injector nozzle and tuned based on the spray measurements like ROI and spray penetration length. Other parameters are set to constant values even for different cases from the relatively simple ECN spray A to the more sophisticated medium-speed DF engine. Also, a sensitivity analysis of the MP ignition model to charge temperature is performed, considering that the experimental data for validation originate from several different test rigs with different boundary conditions. This analysis shows the relationship between the temperature at IVC and ignition delay, which put the precision of the model prediction into perspective with the experimental uncertainties. It is shown that ignition delay is highly sensitive to temperature at IVC since as little as 5 K temperature difference at IVC, which corresponds to roughly 10 K temperature difference at SOI, induce approximately 0.25msec difference in ignition delay, as shown in Fig. 12. In engines, temperature estimation at IVC is quite tricky because of the high turbulent intake flow, heat transfer between wall and charge mixture, and residual burned gas fraction. For this analysis, the tolerance range of ignition delay prediction by the model is set to ± 0.25msec for validation, which indirectly reflects the uncertainty of temperature at IVC ± 5 K.

3.1. ECN spray A: conventional diesel ignition

The MP ignition model is validated using the spray and ignition data measured at the widely accepted and validated Engine Combustion Network (ECN) Spray A conditions and its parametric variations [46]. The ambient conditions tested are similar to charge conditions in diesel engines at the time of injection. The variations of the experimental parameters used for validation in this study include the injection settings (such as injection pressure, injection duration, nozzle exit diameter) and the charge conditions (such as charge density, pressure, temperature, and oxygen concentration), as presented in Table 1.

The spray model input parameters, such as the velocity coefficient and contraction coefficient, are taken from the measured values for the specific injector. Only the model parameter for the spray cone angle is used for tuning. The MP ignition model predicts ignition delay reasonably well for a total of 20 test conditions, as shown in Fig. 13. However, the ignition delay is predicted longer than the measured values for the cases with low charge temperature around 750 K. These deviations come from the charge temperature used for prediction is lower than the actual temperature. In ECN Spray A, the charge temperature corresponds to the local temperature 20 mm away from the nozzle exit in the axial direction. However, these cases have longer spray penetration length before ignition due to the longer ignition delay. As Meijer et al. pointed out, the local temperature within the constant spray chamber of ECN Spray A is varied ± 0.6% compared to the mean temperature due to the wall heat transfer and convection [47]. For instance, it corresponds to the temperature difference of 9 K maximum, which may induce the ignition delay error about 0.5msec.

Table 1
Test conditions for ECN Spray A and its parametric variation.

Injection Pressure	1400–1600 bar
Injection Duration	1.5/6 msec
Nozzle Exit Diameter	84/91 μm
Liquid Fuel	n-dodecane
Charge Density	7–23 kg/m^3
Charge Pressure	20–80 bar
Charge Temperature	750–1200 K
O_2 Concentration	13/15/21%

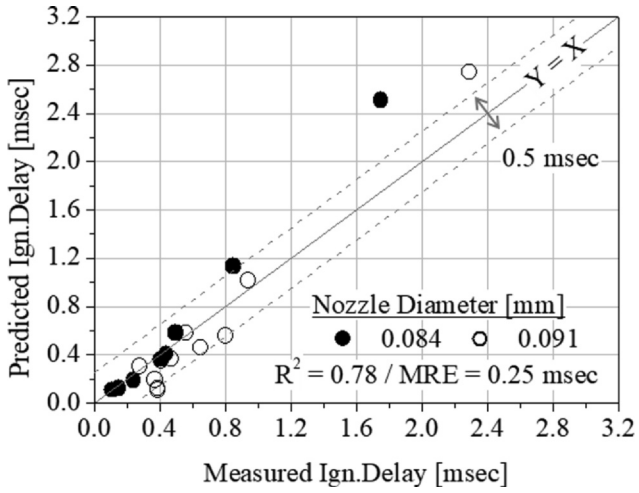

Fig. 13. Ignition delay validation for ECN Spray A.

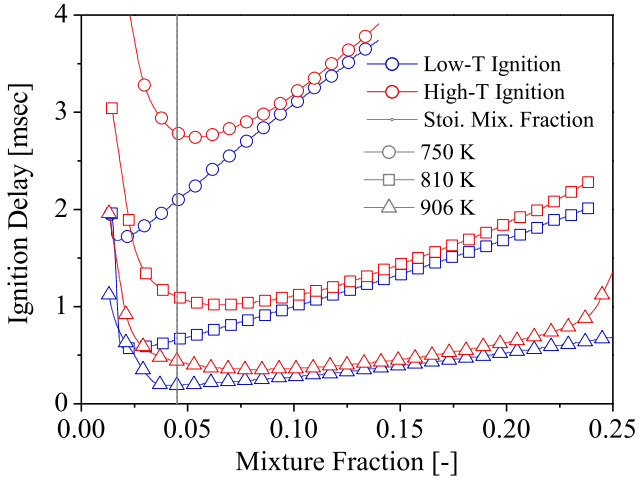

Fig. 14. Ignition delay plot from MP ignition model in mixture fraction space for different ambient temperature conditions in ECN Spray A.

To highlight the sensitivity of ignition to ambient conditions, Fig. 14 shows the ignition delay dependence on the charge temperature and mixture fractions within the spray plume. It clearly shows that higher temperatures reduce the ignition delay significantly. Two-stage diesel ignition is observed for all cases, and it shows a clearer staged ignition for lower temperature cases. LT ignition starts at the leaner condition. On the other hand, high temperature (HT) ignition starts at slightly richer conditions.

The prediction of the ignition location in the conventional diesel engine is validated using optical measurements [48] under the test conditions of charge density 23 kg/m^3, charge temperature 900 K, and injection duration of 1.5msec as shown in Fig. 15. The modeled spray boundary is drawn according to the predicted diesel fuel distribution at the contour of diesel equivalence ratio exceeding 0.1. Contours for LT and HT ignition are drawn along the minimum and maximum ignitable mixture fraction at the specified time. These results being compared to the optical measurements. The LT ignition is detected by CH2O PLIF and, the fuel-jet extent is shown through Schlieren. Schlieren images also indirectly indicate ignition. In the experiment, the LT ignition is identified at 0.24msec aSOI as blurring of the spray boundary since the heat release due to the low-temperature reaction reduces the density difference of fuel-mixture to the surrounding. The HT ignition is identified at 0.39msec aSOI as the Schlieren contrast increases due to the increased density difference between the fuel-mixture and surrounding charge caused by the temperature increase. The model predictions of both the LT and HT ignition are in good agreement with the experiment data, indicating that the model can predict both the spray penetration length and ignition quantitatively well, while it also provides the information about the ignition location. The LT ignition is predicted to start from 0.19msec aSOI along the spray boundary with a specific mixture fraction. Contrary to experimental results, the MP ignition model shows that LT ignition also occurs near nozzle exit since it assumes immediate evaporation of liquid fuel after injection. While this assumption is wrong for long injections, it is believed to be a reasonable assumption for MP ignition because of the short injection duration and long ignition delay. This could be rectified by introducing a liquid part. The liquid length of spray is estimated separately using Elkotb's correlation [49] and demonstrated by the dashed line in Fig. 15. If assuming the liquid part of the spray to be inert, the 1D model would predict LT ignition at 13 mm from the nozzle exit, which is in good agreement with the experimental data. After the start of LT ignition, the LT ignited area rapidly expands within the spray envelope. Next, the HT ignition is observed at 0.34 msec aSOI along the specific mixture fraction boundary within the LT ignited spray envelope, after which it also expands into the rest of the LT ignited spray envelope. However, these ignition areas cannot propagate over the entire spray envelope. The outer boundary becomes too lean to ignite due to over-mixing with the surrounding air, and the inner boundary is too rich to ignite due to the high equivalence ratio of diesel fuel attributed to the long injection duration exceeding the short ignition delay.

3.2. ETH RCEM: MP ignition in methane-air mixtures

The MP ignition model is validated using the spray and ignition data measured under various conditions at the ETH RCEM [50]. The conditions tested are similar to ignition conditions in DF engines. The experimental variations include changes in the injection duration, the air-to-methane ratio of background mixture and, the temperature at SOI, as presented in Table 2. The RCEM tests are especially useful for this study since the experimental conditions include the transient compression process as in engines and short injection duration. Also, optical measurements of spray and ignition are available for model validation.

The spray model parameters such as velocity, area, and spray cone angle coefficients are tuned for the employed injector and kept constant for all experimental conditions. The measured ROI is provided as model input, and the measured spray penetration length is used for validation. The tuned MP ignition model predicts ignition delay reasonably well for a total of 36 test conditions, as shown in Fig. 16. The accuracy of the prediction of ignition delay is also acceptable, especially considering the wide range of conditions and resulting ignition delays. Based on the model results, the effect of the air-to-methane ratio on ignition is highlighted by comparing the modeled LT and HT ignition delay at a different air-to-methane ratio, as shown in Fig. 17. When the injection duration is short, the maximal available diesel fuel concentration rapidly decreases (black line). Therefore, the model shows that the ignition occurs near the maximum mixture fraction line, highlighting the importance of accurately capturing the MP spray evolution.

Furthermore, the ignition delay is increased as the concentration of background methane is increased. The presence of background methane is shown to have two roles in the ignition. First, it increases the LT ignition delay by consuming the intermediate species for diesel ignition, as Schlatter et al. [51] and Srna et al. [52] argued. Second, it makes the propagation of reactions from the ignition spot to fuel-lean mixtures faster. When there is no background methane, the ignition delay at very lean conditions is increasing very sharply. However, the ignition delay shows a smoother increase if the background methane is present. It is thought that the LT ignited background methane increases the local temperature in the very lean spray regions since it contains the extra heating value of methane over the diesel-only case. This effect of methane on the MP ignition is investigated further by model results of LT and HT ignition distribution, which are compared to the optical

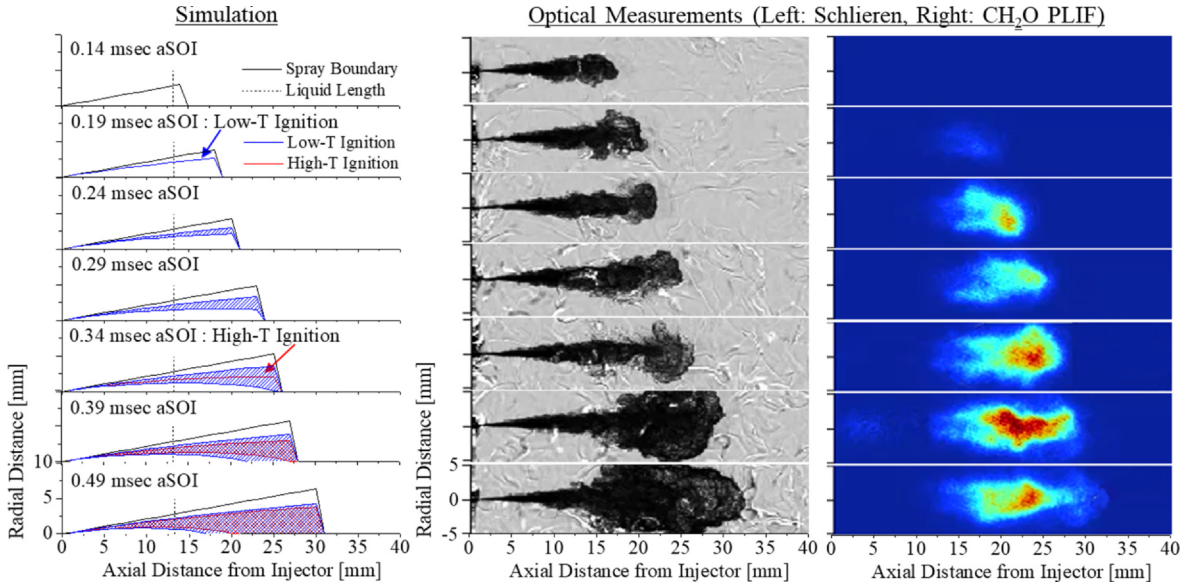

Fig. 15. Simulations and optical measurements of ignition in diesel engine relevant conditions at ECN Spray A (the time of the image panels from the optical measurements and the simulation results correspond to each other).

Table 2
Test conditions for ETH RCEM.

BDC displacement	1.38 dm^3
Stroke	236.5 mm ± 1 mm
Compression ratio	20
Pressure at SOI (P_{SOI})	24 bar
Temperature at SOI (T_{SOI})	772, 814, 860 K
Injection duration	0.40, 0.58, 0.77 msec
Injection pressure	600 bar
Liquid Fuel	n-dodecane
O2 concentration	21%
Air-to-Methane ratio (λ)	1.7/1.9/2.1/Inf.

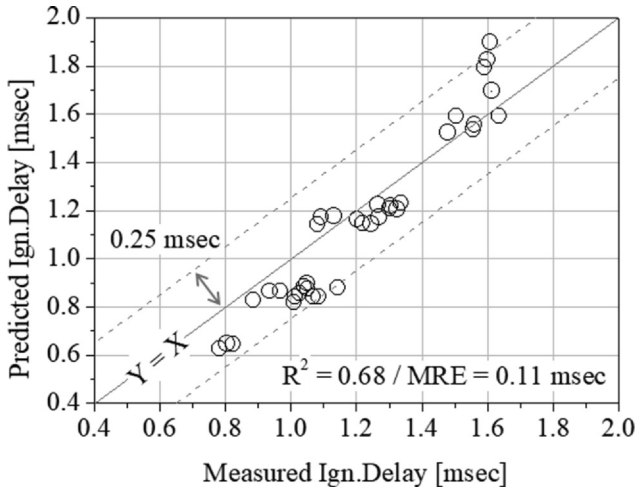

Fig. 16. Ignition delay model validation for ETH RCEM tests.

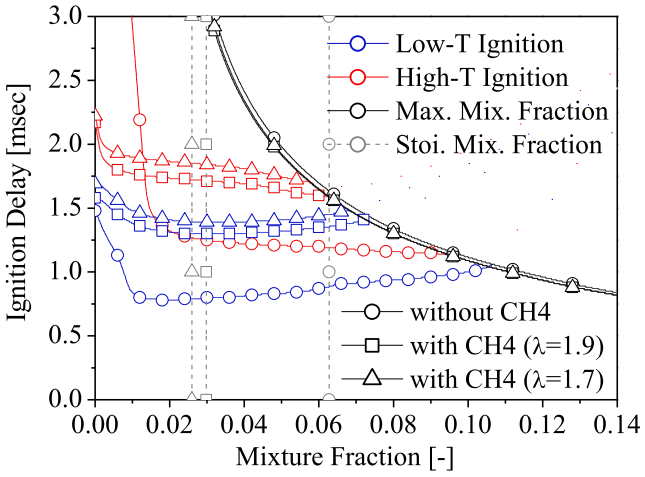

Fig. 17. Ignition delay plot from MP ignition model in mixture fraction space for different background air-to-methane ratio under conditions in the ETH RCEM.

measurements.

First, a case with micro-pilot injection into neat air is investigated by comparing the simulation and the optical measurement [52], as shown in Fig. 18. The experimental settings are the injection duration 0.4msec, the temperature at SOI 772 K, and no presence of background methane. In optical measurements, the optical domain of Schlieren images starts at 22 mm away from the nozzle exit, and the optical domain of CH2O PLIF and OH Chemiluminescence images starts at 15 mm away from the nozzle exit due to the limitation of the experimental test rig. The comparison with the model shows that the MP ignition model can predict the spray penetration length and ignition quantitatively well. The LT ignition is predicted to start from 0.74msec aSOI along the spray boundary with a specific mixture fraction and extends to the nozzle exit both in simulation and optical measurement. After the start of LT ignition, the reacted area rapidly expands to the entire spray envelope, which is aided by the gradual temperature increase due to the compression, unlike in the quasi-stationary ECN spray A case. The HT ignition is experimentally observed at 1.14 msec after SOI at the core region of the spray, where the fuel-richest region within the spray is located. Afterward, combustion rapidly expands into the spray envelope, as indicated by the consumption of CH2O. However, the HT ignition cannot propagate over the entire spray envelope since the outer boundary becomes too lean to ignite due to over-mixing with the surrounding air. These over-mixing regions also present near the nozzle exit as the air is entrained after the end of the injection. This is visible as the remaining weak CH2O signal at the contour of the jet, as correctly reproduced by the model as well.

Second, the modeled ignition evolution in a case with background methane is compared to the optical measurement [52], as shown in

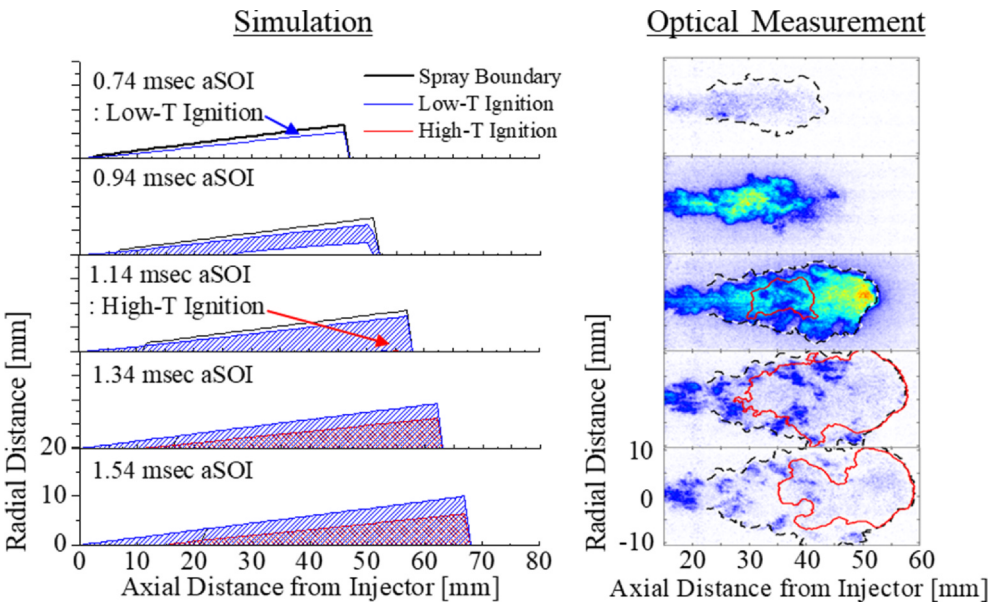

Fig. 18. MP ignition simulation compared to the optical measurement at ETH RCEM conditions without background methane (In optical measurement, the colored contour is CH2O PLIF images, black dashed line is the boundary of Schlieren images, and the solid red line is the boundary of OH images. The time instants of the image panels of the optical measurements and the simulation results correspond to each other). (For interpretation of the references to colour in this figure legend, the reader is referred to the web version of this article.)

Fig. 19. The conditions are kept constant as the previous case except for the presence of background methane with the air-to-methane ratio (λ) of 1.7. This case can be seen to be quite representative of a medium-speed DF engine, except there is no turbulence within the combustion chamber of employed RCEM. One can see that the MP ignition model can predict the spray penetration length and ignition quantitatively well. The model predicts the LT ignition to start from 1.34msec aSOI along the spray boundary with a specific mixture fraction, followed by a rapid expansion of the reacted area throughout the entire spray envelope within 0.2msec, which is faster than in the previous non-methane case. Also, the LT ignition propagates outside of the spray envelope with an equivalence ratio of 0.1, which is located between the nozzle exit and the trailing edge of the spray. This attributed to the presence of methane. The HT ignition is observed at 1.74 msec aSOI at the core region of the spray, where the richest region within the spray is located, and, similarly to the LT ignition, it rapidly expands within the spray envelope. Unlike the previous case, the HT ignition expands to the entire LT ignition region. As a consequence, the flame surface area becomes larger than in the non-methane case, as visible from the comparison of the optical measurements.

3.3. Medium-speed dual-fuel engine

The MP ignition model is validated using the test data measured at a medium-speed DF engine with specifications shown in Table 3. During the gas operation mode, the DF engine is fueled with natural gas (city gas, more than 98% of the total fuel energy) supplied at the intake port, which is designed to form a homogeneous charge with a lean air-methane mixture in the cylinder. Then, a small amount of diesel fuel (MGO, usually 0.5 to 2% of the total fuel energy) is injected directly into the cylinder through the MP injector for the ignition. The engine tests are performed under the various test conditions, such as charge conditions, injection pressure, duration of injection, and air-to-methane ratios shown in Table 3. In addition, two different compression ratio of the engine is tested; Configuration A has a compression ratio of 13.5 and, configuration B has a compression ratio of 12.7. The ignition delay is defined as the time between the injection timing and the start of combustion. Here, the start of combustion is obtained from the heat

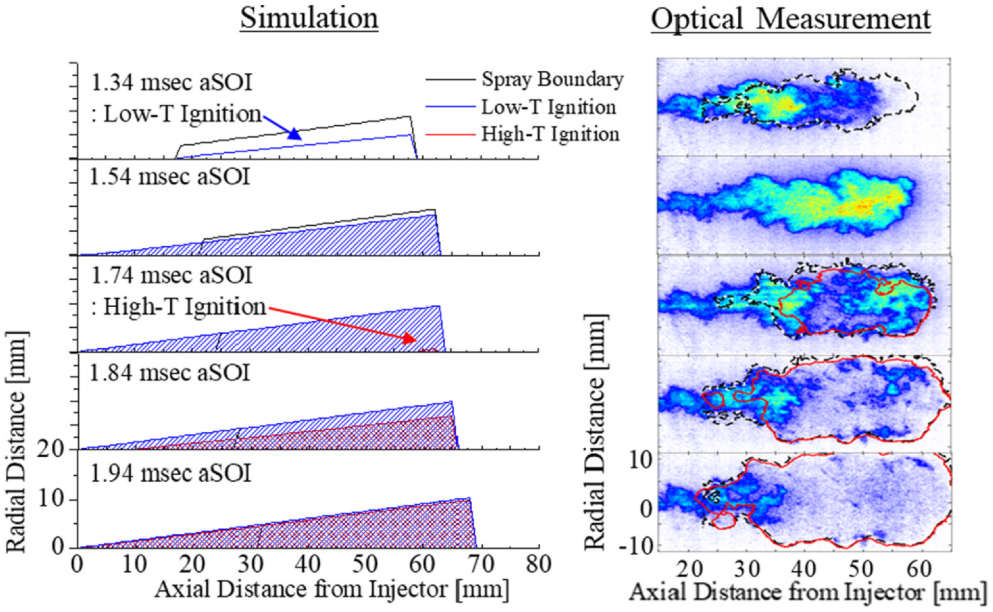

Fig. 19. MP ignition simulation compared to the optical measurement at ETH RCEM conditions with background methane (λ = 1.7) (In optical measurement, the colored contour is CH2O PLIF images, black dashed line is the boundary of Schlieren images, and the solid red line is the boundary of OH images. The time instants of the image panels of the optical measurements and the simulation results correspond to each other). (For interpretation of the references to colour in this figure legend, the reader is referred to the web version of this article.)

Table 3
Test conditions for a medium-speed DF engine.

Bore/Stroke	350/400 mm	Gas Operation	- Micro-pilot ignited Otto Cycle
Rated Speed	720 rpm		- Main Fuel (99%): City Gas
BMEP	20.8 bar		- Pilot Fuel (~1%): MGO/MDO
Pressure at SOI	31–82 bar		- Low-Pressure Gas System
Temperature at SOI	650–835 K	Diesel Operation	- Conventional Diesel Cycle
Injection Pressure	1000 bar		- Main Fuel: MGO/MDO/HFO
Injection Duration	0.7–2.2 msec		- Conventional Fuel Oil System
Air-to-Methane Ratio (λ)	1.8–2.2		

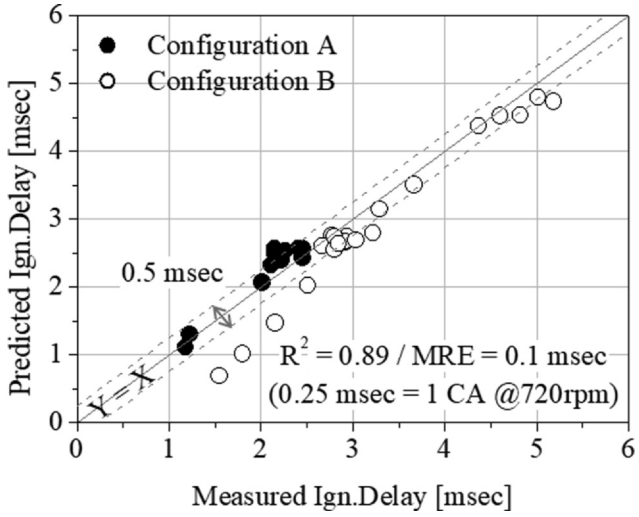

Fig. 20. Ignition delay validation for a medium-speed DF engine.

release rate, which is calculated from the measured combustion pressure. The model is validated for a total of 36 test conditions, as shown in Fig. 20. The MP ignition model predicts the ignition delay within reasonable accuracy, considering the wide range of the test conditions and difficulties in estimating the local temperatures within the cylinder.

The ignition delay in the DF engine test ranges from 1 to 5msec, which corresponds to 4.3 and 21.6CAdeg at a speed of 720 rpm, respectively. These ignition delays are longer and broader than previous test cases from ECN Spray A or ETH RCEM since the temperature at SOI in the DF engine is lower and has a broader range (650–835 K). The MP ignition process is investigated further in Fig. 21. The investigated representative conditions for the medium-speed DF engine are chosen as follows: the compression ratio 13.5, the pressure at SOI 49 bar, the temperature at SOI 723 K, the background air-to-methane ratio (λ) of 1.8, the injection duration of 1msec and the injection pressure of 1000 bar. The MP ignition shows similar characteristics as in the previously studied ETH RCEM case with the DF engine similar condition. The LT ignition starts at 2.13msec aSOI along the specific mixture fraction boundary of the spray. Then, it propagates rapidly into the entire spray envelope within 0.3msec. The HT ignition starts at 2.39msec aSOI and, it also spread rapidly over the entire LT reacted region.

4. Parameter studies on DF engine

The MP ignition model is used to investigate the effects of the various engine operating parameters on the ignition in the medium-speed DF engine. The base case for the parameter study is the case presented in Fig. 21, and the parameter studies are performed by changing one parameter per each case while keeping the other parameter values. The injection timing, injection duration, injection pressure, injector nozzle diameter, and air-to-fuel ratio are chosen as parameters to be varied.

The ignition diagrams for each parameter study are shown in Fig. 22. Advancing the injection timing significantly increases the ignition delay since the temperature and pressure at SOI are decreased accordingly. Also, advanced SOI decreases the range of ignitable mixture fraction by increasing the time for spray mixing with the surrounding mixture. Longer injection duration secures higher SDR due to the spray induced turbulence. Consequently, the ignition delay is slightly reduced since the higher SDR promotes mixing between the diesel fuel and background mixture. Higher injection pressure keeping the same mass of diesel fuel shows the slightly longer ignition delay as it causes the shorter injection duration. Larger nozzle diameter keeping the same mass of diesel fuel shows the minor effect on ignition delay as

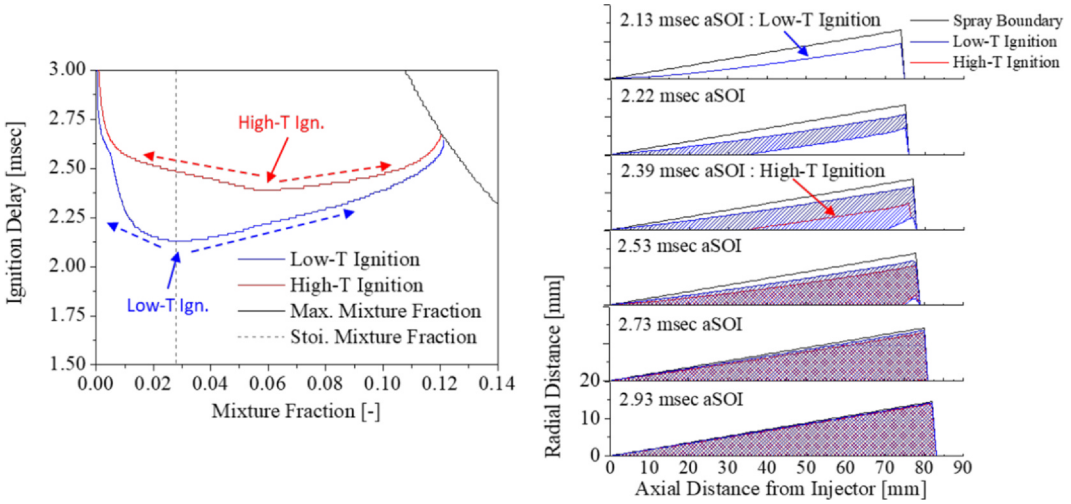

Fig. 21. Ignition delay diagram from the MP ignition model in mixture fraction space (Left) and Spray and ignition contours (Right) for a representative condition in a medium-speed DF engine.

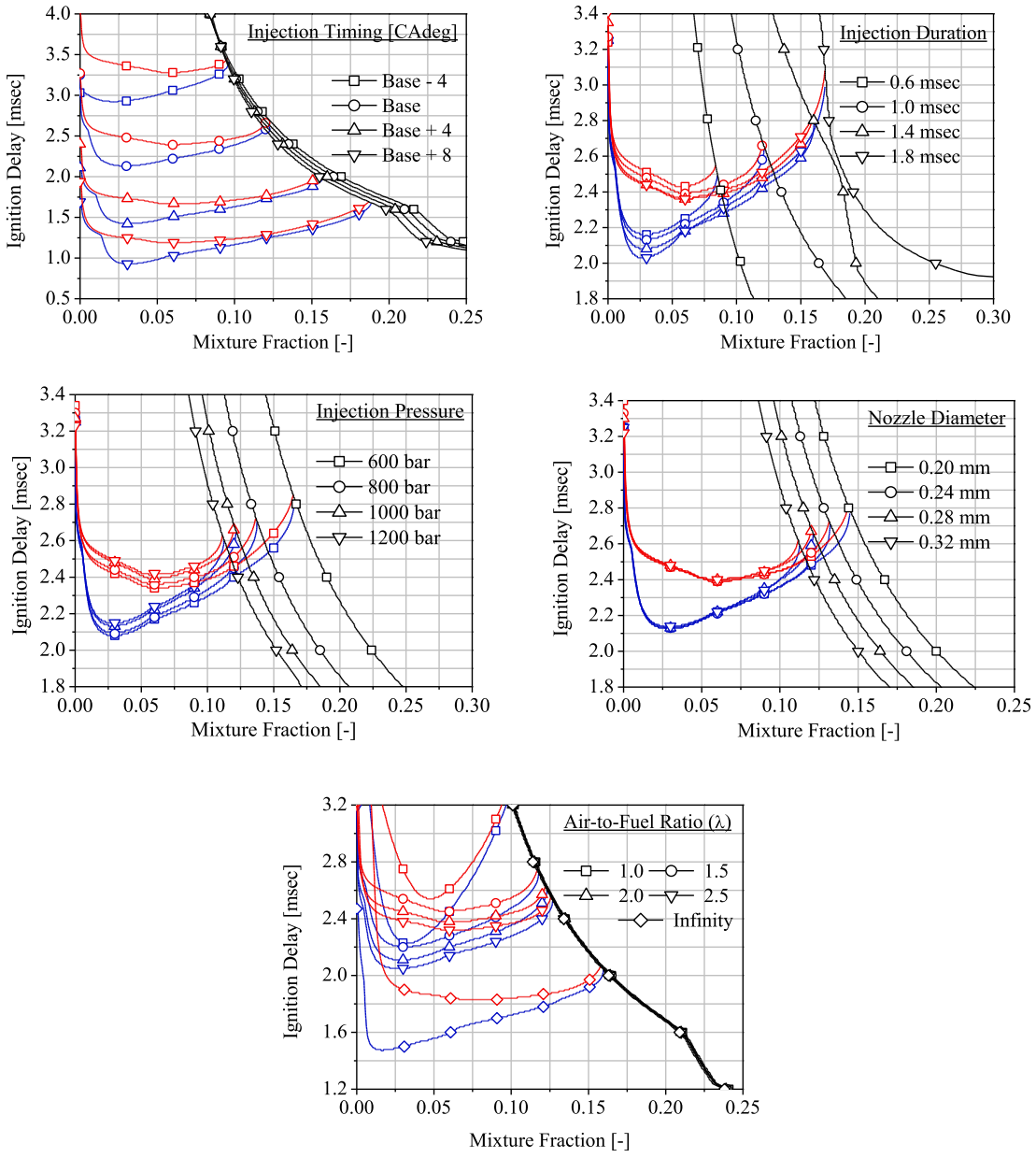

Fig. 22. Parameter studies for MP ignition in medium-speed DF engine (red: HT ignition delay, blue: LT ignition delay, black: maximum mixture fraction within the spray plume). (For interpretation of the references to colour in this figure legend, the reader is referred to the web version of this article.)

it causes the shorter injection duration and the larger spray cone angle, which are compensating their effect on SDR each other. Though there is only a slight difference in ignition delay when varying the injection pressure or nozzle diameter, the spray penetration length can have a relatively larger difference, and it makes the different ignition locations that affect the subsequent combustion process. Richer background methane concentration induces longer ignition delay and more stable ignition at a very lean spray envelope. However, the ignition becomes unstable when the background methane concentration reaches stoichiometry as the methane consumes the intermediate products needed for the HT ignition of diesel fuel.

5. Conclusions

In this paper, a novel phenomenological MP ignition model for a medium-speed DF engine is developed. The spray submodel is tailored to deal with the transition period of MP spray by adopting the trapezoidal ROI, variable contraction coefficient for the nozzle, and the turbulence term. The main spray characteristics such as spray penetration length, distribution of fuel fraction, and SDR are predicted with precision. The chemistry submodel using the 0D flamelet model based on the opposed flow reactor is adapted with a detailed chemical mechanism for n-dodecane. This approach allows the interaction between turbulence and chemistry, which is essential for the ignition in an MP spray. The developed MP ignition model requires only three tuning parameters, which are reflecting the injector nozzle geometry. Other parameters are set to constant values even for different cases from the relatively simple ECN spray A to the more sophisticated medium-speed DF engine.

The model is validated against test data, including the optical measurements from the ECN Spray A and a rapid compression and expansion machine, as well as pressure data from the multi-cylinder medium-speed DF engine. The MP ignition model predicts the ignition delay and ignition location precisely from the conventional diesel ignition to the MP ignition in DF engines. Calculation results are introduced in two graphical ways for further investigations: Ignition

delay graphs in mixture fraction space, and temporal evolutions of spray, LT and HT ignition boundaries in 2D crosscut along the axial direction. These plots are used for the qualitative characterization of combustion and ignition stability. The MP ignition model identifies the different ignition processes observed depending on the conditions.

1) Conventional diesel ignition:

The LT and HT ignition cannot be expanded over the entire spray envelope. The outer boundary becomes too lean to ignite due to overmixing with the surrounding air, and the inner boundary becomes too rich to ignite due to the oversupplied diesel fuel due to the long injection duration and short ignition delay.

2) MP ignition in DF engines without background methane:

The HT ignition starts at the most reactive region within the spray, the center of the spray tip region, and it expands rapidly into the spray envelope. However, the reacted region does not expand over the entire spray envelope since the outer boundary becomes too lean to ignite due to the overmixing with the surrounding air. Even more, it contracts toward the spray downstream because of the air entrainment from the nozzle exit region after the end of injection.

3) MP ignition in DF engines with background methane:

The LT ignition is delayed compared to the non-methane case. However, the LT ignition spreads over the entire spray envelope faster, and it even expands outside of the spray envelope due to the presence of methane. The HT ignition starts at the center of the spray tip region, and it expands rapidly into the entire LT ignited region. As a consequence, the flame surface area becomes larger than in the non-methane case. The presence of methane is shown to have two roles in the MP ignition. First, it increases the ignition delay by retarding the LT reactions. Second, it makes the propagation of reactions from the ignition spots to fuel-lean mixtures faster.

The MP ignition model developed in this study shows good agreement with the various measurement campaigns, especially for the ignition delay and ignition location with minimum tuning parameters. The model is expected to be utilized for the medium-speed DF engine development for the design of the combustion system and its operating ranges, as shown in the parameter studies, for instance. Furthermore, the model would serve as a sound basis for the development of the subsequent DF combustion model.

CRediT authorship contribution statement

Hyunchun Park: Conceptualization, Methodology, Software, Validation, Formal analysis, Investigation, Writing - original draft, Visualization. **Yuri M. Wright:** Writing - review & editing, Supervision. **Omar Seddik:** Writing - review & editing, Investigation. **Ales Srna:** Writing - review & editing, Investigation, Visualization. **Panagiotis Kyrtatos:** Conceptualization, Writing - review & editing, Supervision. **Konstantinos Boulouchos:** Writing - review & editing, Supervision.

Declaration of Competing Interest

The authors declare that they have no known competing financial interests or personal relationships that could have appeared to influence the work reported in this paper.

Acknowledgments

The authors would like to acknowledge the financial support of the Swiss Competence Centre for Energy Research (SCCER Mobility), the Swiss Federal Office of Energy, and Hyundai Heavy Industries Co., Ltd.

References

[1] CIMAC WG17 Gas Engines. Information concerning the application of gas engines in the marine industry. CIMAC Position Pap 2013.
[2] Hoff M, Sturm M, Graumueller R, Rickert C. Optimization of the dual-fuel MicroPilot combustion process for commercial applications. CIMAC Congr 2019;2019:p. No.258.
[3] CIMAC WG17 Gas Engines. Gas Engine Aftertreatment Systems. CIMAC Position Pap; 2017.
[4] García Valladolid P, Tunestål P, Monsalve-Serrano J, García A, Hyvönen J. Impact of diesel pilot distribution on the ignition process of a dual fuel medium speed marine engine. Energy Convers Manage 2017;149:192–205. https://doi.org/10.1016/j.enconman.2017.07.023.
[5] Marten C, Werner B, Ghetti S, Sven L, Thorenz C, Heusery P. Variable compression ratio technology for dual-fuel engines. CIMAC Congr 2019;2019. p. No.257.
[6] Musculus MPB, Miles PC, Pickett LM. Conceptual models for partially premixed low-temperature diesel combustion. Prog Energy Combust Sci 2013. https://doi.org/10.1016/j.pecs.2012.09.001.
[7] Kundu P, Ameen MM, Som S. Importance of turbulence-chemistry interactions at low temperature engine conditions. Combust Flame 2017. https://doi.org/10.1016/j.combustflame.2017.05.025.
[8] Srna A, Bolla M, Wright YM, Herrmann K, Bombach R, Pandurangi SS, et al. Effect of methane on pilot-fuel auto-ignition in dual-fuel engines. Proc Combust Inst 2019. https://doi.org/10.1016/j.proci.2018.06.177.
[9] Schlatter S, Schneider B, Wright YM, Boulouchos K. Comparative study of ignition systems for lean burn gas engines in an optically accessible rapid compression expansion machine. SAE Tech Pap 2013;6. https://doi.org/10.4271/2013-24-0112.
[10] Barro C, Seddik O, Wright YM, Pandurangi S, Kyrtatos P, Boulouchos K. Investigation of the ignition process of pilot injections using CFD. SAE Tech Pap 2019. https://doi.org/10.4271/2019-24-0129.
[11] Malbec LM, Eagle WE, Musculus MPB, Schihl P. Influence of injection duration and ambient temperature on the ignition delay in a 2.34L optical diesel engine. SAE Int J Engines 2015;9:47–70. https://doi.org/10.4271/2015-01-1830.
[12] Musculus MPB, Lachaux T, Pickett LM, Idicheria CA. End-of-injection over-mixing and unburned hydrocarbon emissions in low-temperature-combustion diesel engines. SAE Tech Pap 2007. https://doi.org/10.4271/2007-01-0907.
[13] Park H, Kyrtatos P, Bolla M, Lee Y, Yoon W, Boulouchos K. Combustion modeling of a medium-speed dual-fuel engine using double Vibe function. CIMAC Congr 2019;20192. p. No.019.
[14] Soriano BS, Richardson ES, Schlatter S, Wright YM. Conditional moment closure modelling for dual-fuel combustion engines with pilot-assisted compression ignition. SAE Tech Pap 2017;2017. https://doi.org/10.4271/2017-01-2188.
[15] Kahila H, Wehrfritz A, Kaario O, Vuorinen V. Large-eddy simulation of dual-fuel ignition: Diesel spray injection into a lean methane-air mixture. Combust Flame 2019. https://doi.org/10.1016/j.combustflame.2018.10.014.
[16] Frühhaber J, Peter A, Schuh S, Lauer T, Wensing M, Winter F, et al. Modeling the pilot injection and the ignition process of a dual fuel injector with experimental data from a combustion chamber using detailed reaction kinetics. SAE Tech Pap 2018. https://doi.org/10.4271/2018-01-1724.
[17] Seddik O, Pandurangi S, Bolla M, Boulouchos K, Srna A, Wright YM. Flamelet generated manifolds applied to Dual-Fuel combustion of lean methane/air mixtures at engine relevant conditions ignited by n dodecane micro pilot sprays. SAE Tech Pap 2019. https://doi.org/10.4271/2019-01-1163.
[18] Eder L, Ban M, Pirker G, Vujanovic M, Priesching P, Wimmer A. Development and validation of 3D-CFD injection and combustion models for dual fuel combustion in diesel ignited large gas engines. Energies 2018. https://doi.org/10.3390/en11030643.
[19] Xu S, Anderson D, Hoffman M, Prucka R, Filipi Z. A phenomenological combustion analysis of a dual-fuel natural-gas diesel engine. Proc Inst Mech Eng Part D J Automob Eng 2017. https://doi.org/10.1177/0954407016633337.
[20] Cernik F, Macek J, Dahnz C, Hensel S. Dual fuel combustion model for a large low-speed 2-stroke engine. SAE Tech Pap 2016. https://doi.org/10.4271/2016-01-0770.
[21] Musculus MPB, Kattke K. Entrainment waves in diesel jets. SAE Tech Pap 2009;2:1170–93. https://doi.org/10.4271/2009-01-1355.
[22] Barro C, Nani C, Hutter R, Boulouchos K. Spray model based phenomenological combustion description and experimental validation for a dual fuel engine. SAE Tech Pap 2017. https://doi.org/10.4271/2017-24-0098.
[23] Frerichs J, Eilts P. Development of a physically/chemically based approach for 2-stage ignition delay calculation in medium speed dual-fuel engines. SAE Tech Pap 2019. https://doi.org/10.4271/2019-24-0068.
[24] Krishnan SR, Srinivasan KK, Midkiff KC. Phenomenological modeling of low-temperature advanced low pilot-ignited natural gas combustion. SAE Tech Pap 2007;2007:776–90. https://doi.org/10.4271/2007-01-0942.
[25] Taritas I, Kozarac D, Sjeric M, Sierra Aznar M, Vuilleumier D, Tatschl R. Development and validation of a quasi-dimensional dual fuel (diesel – natural gas) combustion model. SAE Int J Engines 2017;10:483–500. https://doi.org/10.4271/2017-01-0517.
[26] Krenn M, Pirker G, Wimmer A, Djuranec S, Meier MC, Waldenmaier U, et al. Methodology for analysis and simulation of dual fuel combustion in large engines. THIESEL 2014 Conf Thermo- Fluid Dyn Process Direct Inject Engines 2014:1–14.
[27] Kozarac D, Taritas I, Sjeric M, Krajnovic J, Sremec M. The optimization of the dual fuel engine injection parameters by using a newly developed quasi-dimensional

cycle simulation combustion model. SAE Tech Pap 2018;2018. https://doi.org/10.4271/2018-01-0261.
[28] Krenn M, Redtenbacher C, Pirker G, Wimmer A. A new approach for combustion modeling of large dual-fuel engines; 2018. https://doi.org/10.1007/978-3-658-21583-5_11.
[29] Bolla M, Farrace D, Wright YM, Boulouchos K, Mastorakos E. Influence of turbulence-chemistry interaction for n-heptane spray combustion under diesel engine conditions with emphasis on soot formation and oxidation. Combust Theory Model 2014. https://doi.org/10.1080/13647830.2014.898795.
[30] Naber JD, Siebers DL. Effects of gas density and vaporization on penetration and dispersion of diesel sprays. SAE Tech Pap 1996. https://doi.org/10.4271/960034.
[31] Siebers DL. Scaling liquid-phase fuel penetration in diesel sprays based on mixing-limited vaporization. SAE Tech Pap 1999. https://doi.org/10.4271/1999-01-0528.
[32] Abramovich GN. The Theory of Turbulent Jets. Cambridge, MA, USA: MIT Press; 1963.
[33] Pastor JV, Javier López J, García JM, Pastor JM. A 1D model for the description of mixing-controlled inert diesel sprays. Fuel 2008. https://doi.org/10.1016/j.fuel.2008.04.017.
[34] Park J, Jang JH, Park S. Effect of fuel temperature on heavy fuel oil spray characteristics in a common-rail fuel injection system for marine engines. Ocean Eng 2015. https://doi.org/10.1016/j.oceaneng.2015.06.002.
[35] Moon S, Huang W, Li Z, Wang J. End-of-injection fuel dribble of multi-hole diesel injector: Comprehensive investigation of phenomenon and discussion on control strategy. Appl Energy 2016. https://doi.org/10.1016/j.apenergy.2016.06.116.
[36] Salvador FJ, Martínez-López J, Caballer M, De Alfonso C. Study of the influence of the needle lift on the internal flow and cavitation phenomenon in diesel injector nozzles by CFD using RANS methods. Energy Convers Manage 2013. https://doi.org/10.1016/j.enconman.2012.10.011.
[37] Pozorski J, Sazhin S, Wacławczyk M, Crua C, Kennaird D, Heikal M. Spray penetration in a turbulent flow. Flow Turbul Combust 2002;68:153–65. https://doi.org/10.1023/A:1020497028986.
[38] Peters N, Kanury A. Turbulent combustion. Appl Mech Rev 2001. https://doi.org/10.1115/1.1383686.
[39] O'Brien EE, Jiang TL. The conditional dissipation rate of an initially binary scalar in homogeneous turbulence. Phys Fluids A 1991. https://doi.org/10.1063/1.858127.
[40] Pitsch H. Unsteady flamelet modeling of differential diffusion in turbulent jet diffusion flames. Combust Flame 2000. https://doi.org/10.1016/S0010-2180(00)00135-8.
[41] Mehl M, Pitz WJ, Westbrook CK, Curran HJ. Kinetic modeling of gasoline surrogate components and mixtures under engine conditions. Proc Combust Inst 2011. https://doi.org/10.1016/j.proci.2010.05.027.
[42] Liu S, Hewson JC, Chen JH, Pitsch H. Effects of strain rate on high-pressure nonpremixed n-heptane autoignition in counterflow. Combust Flame 2004. https://doi.org/10.1016/j.combustflame.2004.01.011.
[43] Ranzi E, Frassoldati A, Stagni A, Pelucchi M, Cuoci A, Faravelli T. Reduced kinetic schemes of complex reaction systems: fossil and biomass-derived transportation fuels. Int J Chem Kinet 2014. https://doi.org/10.1002/kin.20867.
[44] Pei Y, Mehl M, Liu W, Lu T, Pitz WJ, Som S. A multicomponent blend as a diesel fuel surrogate for compression ignition engine applications. J Eng Gas Turbines Power 2015. https://doi.org/10.1115/1.4030416.
[45] Hockett AG, Hampson G, Marchese AJ. Natural gas/diesel RCCI CFD simulations using multi-component fuel surrogates. Int J Powertrains 2017. https://doi.org/10.1504/IJPT.2017.082915.
[46] Engine Combustion Network (ECN). Online 2019. https://ecn.sandia.gov/ecn-data-search/.
[47] Meijer M, Somers B, Johnson J, Naber J, Lee SY, Malbec LM, et al. Engine combustion network (ECN): characterization and comparison of boundary conditions for different combustion vessels. At Sprays 2012. https://doi.org/10.1615/AtomizSpr.2012006083.
[48] Skeen SA, Manin J, Pickett LM. Simultaneous formaldehyde PLIF and high-speed schlieren imaging for ignition visualization in high-pressure spray flames. Proc Combust Inst 2015. https://doi.org/10.1016/j.proci.2014.06.040.
[49] Elkotb MM. Fuel atomization for spray modelling. Prog Energy Combust Sci 1982. https://doi.org/10.1016/0360-1285(82)90009-0.
[50] Srna A, von Rotz B, Herrmann K, Boulouchos K, Bruneaux G. Experimental investigation of pilot-fuel combustion in dual-fuel engines, Part 1: Thermodynamic analysis of combustion phenomena. Fuel 2019. https://doi.org/10.1016/j.fuel.2019.115642.
[51] Schlatter S, Schneider B, Wright YM, Boulouchos K. N-heptane micro pilot assisted methane combustion in a Rapid Compression Expansion Machine. Fuel 2016. https://doi.org/10.1016/j.fuel.2016.03.006.
[52] Srna A, von Rotz B, Bolla M, Wright YM, Herrmann K, Boulouchos K, et al. Experimental investigation of pilot-fuel combustion in dual-fuel engines, Part 2: Understanding the underlying mechanisms by means of optical diagnostics. Fuel 2019;255:115766https://doi.org/10.1016/j.fuel.2019.115766.